

Imaging the Nonlinear Plasmoemission Dynamics of Electrons from Strong Plasmonic Fields

Daniel Podbiel,^{*,†} Philip Kahl,[†] Andreas Makris,[†] Bettina Frank,[‡] Simon Sindermann,[†] Timothy J. Davis,^{‡,§} Harald Giessen,[‡] Michael Horn-von Hoegen,[†] and Frank-J. Meyer zu Heringdorf^{*,†}

[†]Faculty of Physics and CENIDE, University of Duisburg-Essen, Lotharstr. 1, 47057 Duisburg, Germany

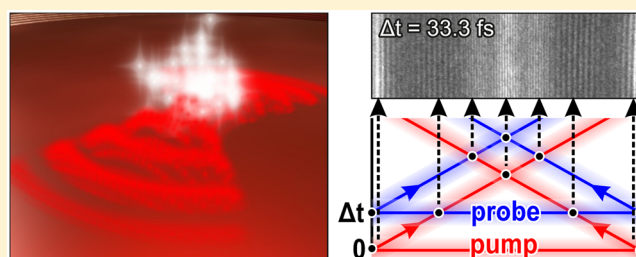
[‡]Fourth Physics Institute and Research Center SCoPE, University of Stuttgart, Pfaffenwaldring 57, 70550 Stuttgart, Germany

[§]School of Physics, University of Melbourne, Parkville, Victoria 3052, Australia

S Supporting Information

ABSTRACT: We use subcycle time-resolved photoemission microscopy to unambiguously distinguish optically triggered electron emission (photoemission) from effects caused purely by the plasmonic field (termed “plasmoemission”). We find from time-resolved imaging that nonlinear plasmoemission is dominated by the transverse plasmon field component by utilizing a transient standing wave from two counter-propagating plasmon pulses of opposite transverse spin. From plasmonic foci on flat metal surfaces, we observe highly nonlinear plasmoemission up to the fifth power of intensity and quantized energy transfer, which reflects the quantum-mechanical nature of surface plasmons. Our work constitutes the basis for novel plasmonic devices such as nanometer-confined ultrafast electron sources as well as applications in time-resolved electron microscopy.

KEYWORDS: Time-resolved photoemission microscopy, plasmoemission, surface plasmon polariton, photoemission, above-threshold photoemission



Ever since the first quantum-mechanical explanation of the photoelectric effect by Einstein, light-induced emission of electrons from metallic surfaces has been an intensively studied phenomenon.^{1–5} It was discovered that plasmonic resonances can dramatically increase the photoemission yield,^{6,7} and recently it was found that plasmonic near-field enhancements may drive systems even into the strong-field regime.^{8–12} A clear distinction between electron emission from *optical* and *plasmonic* fields, however, was not possible until now.^{13,14}

Surface plasmons are electron density oscillations that exist at the interface between a metal and its dielectric surrounding. Light can couple to such plasmons and induce large local electric fields, forming surface plasmon polaritons. If the field strength is high enough, several photons can combine their energies and enable electrons to exceed the work function of the surface, thus causing photoemission. Among other techniques like scanning near field optical microscopy (SNOM),^{15,16} leakage-field radiation microscopy (LFRM),^{17,18} or cathodoluminescence scanning transmission electron microscopy (STEM-CL),¹⁹ time-resolved photoemission microscopy (PEEM) has been utilized to image propagating surface plasmons.^{20–23} Surface plasmon interference,^{24,25} surface plasmon dispersion,²³ surface plasmon focusing,²⁶ and plasmon routing,^{27,28} as well as localized plasmons in restricted nm-sized geometries^{11,29,30} have been observed. Also, PEEM has been utilized to image short-range

plasmon propagation as well as plasmonic focusing³¹ and plasmonic orbital angular momentum dynamics.³²

However, in all of these experiments, it was debatable whether the electron emission originated from the light field or rather from plasmons directly. Mershdorf has pointed out more than 15 years ago that several excitation pathways can result in the liberation of a photoelectron.³³

Here, we add an important new dimension to photoemission science from nanostructured metallic surfaces by imaging the dynamics of *nonlinear plasmoemission*, which represents the decay of a collective excitation of the electronic system to a single electron and subsequent emission of this electron. We utilize space-time domain electron emission microscopy to distinguish *optical* from *plasmonic* emission and demonstrate processes where up to five plasmons simultaneously cause the emission of a single electron of high energy. We detect the liberated electrons with spatial and energy resolution.

Figure 1a shows a sketch of the experimental setup. The linearly polarized laser pulses (800 nm, 1.55 eV) impinge on the sample along the surface normal. The electrons emitted from the sample are projected onto a detector. The acquisition time of the detector is of the order of seconds; that is, the image

Received: May 27, 2017

Revised: September 16, 2017

Published: September 25, 2017

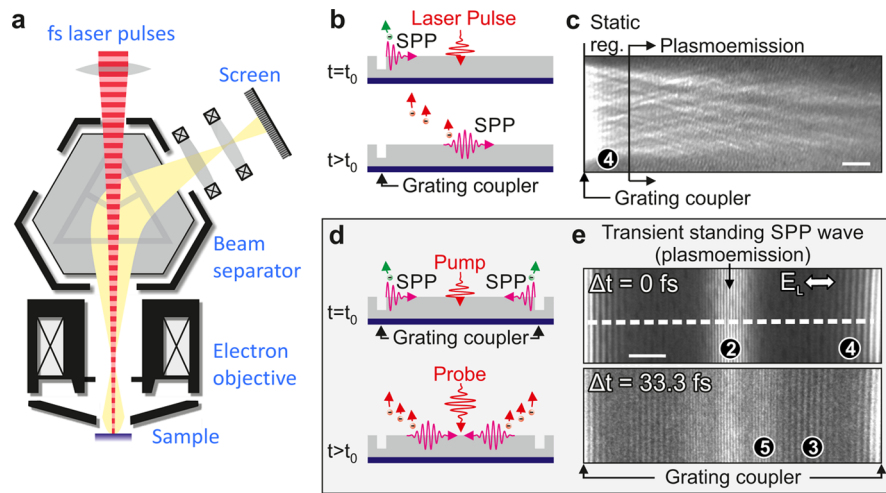


Figure 1. Experimental observation of plasmoemission. (a) Sketch of the experimental setup. (b, d) Illustrations of the experiments, side view. (c, e) 2PPE PEEM images, top view, scale bars correspond to 5 μm . (b, c) A laser pulse excites a propagating SPP pulse at a linear grating coupler. During its propagation across the surface, the SPP decays and excites electrons that are emitted. (d, e) Two laser pulses excite two counter-propagating SPPs at two linear grating couplers. The SPPs are probed and interfere with each other, resulting in the signatures (3, 4) and (2, 5), respectively. A systematic numbering of the signatures is discussed in the context of Figure 2 and in the Supporting Information (Figure S1).

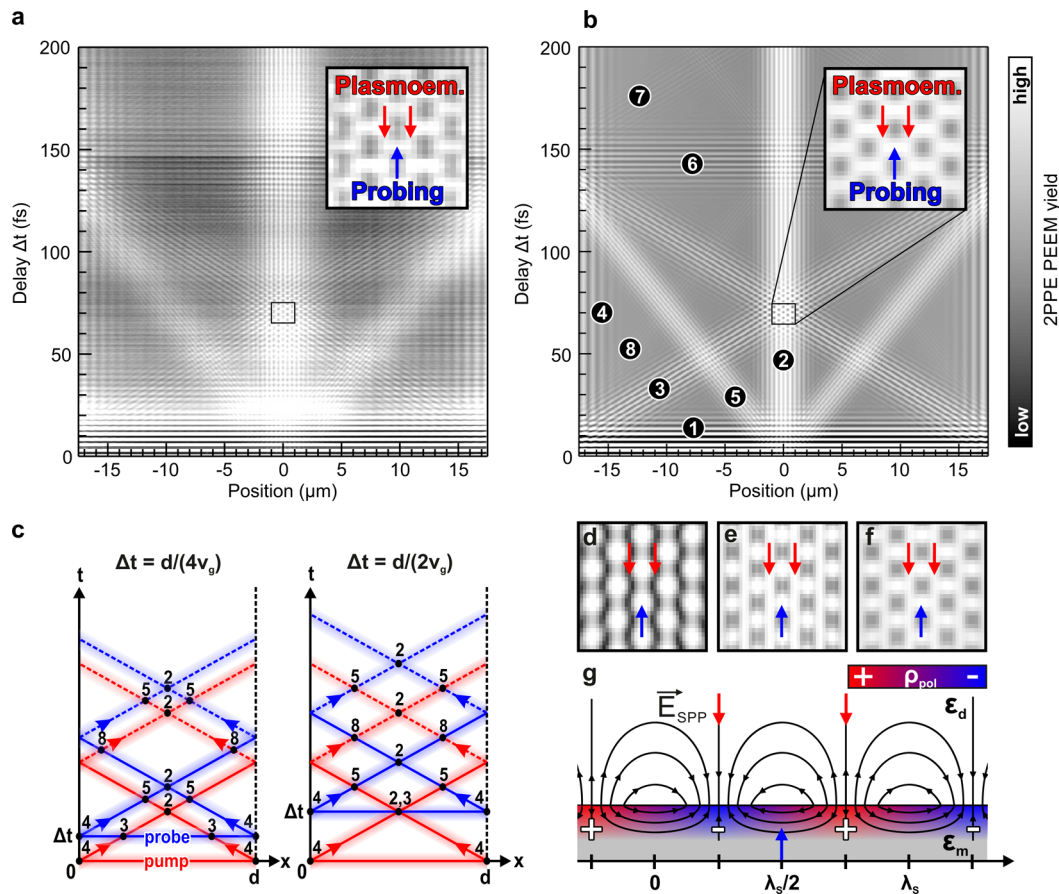


Figure 2. Analysis of the measurement signatures and transient standing SPP wave. (a, b) Stack of line profiles along the dashed horizontal white line in Figure 1e for different delays Δt between the laser pulses. (a) Experimental result. (b) Simulation result based on eq 1 with $\alpha = 5.8$, $\beta^2/\alpha^2 = 2$ considering the fields at the interface inside the metal. (c) Concept of spatiotemporal overlap illustrated by “space-time diagrams” for two different delays Δt . (d, e, f) Simulation results for the inset region with (d) $\alpha = 1$, $\beta^2/\alpha^2 = 2$, (e) $\alpha = 5.8$, $\beta = 0$, and (f) $\alpha = 5.8$, $\beta^2/\alpha^2 = 1$. (g) Electric field and corresponding polarization charge density ρ_{pol} of a (standing) SPP wave at a fixed time.

acquisition is time-integrated and accumulated over a large number of pulses.

Figure 1b,c illustrates the contrast formation process. As sketched in Figure 1b, a fs laser pulse impinges on the surface

and excites a fs SPP pulse at a linear grating coupler, which propagates across the surface. Figure 1c shows a typical two-photon photoemission (2PPE) based PEEM image from the vicinity of a linear grating coupler in a polycrystalline Ag film

after lowering the work function by Cs. During the first 20 fs of propagation, the SPP is coherently probed by the same laser pulse that excited the SPP. Interference between the laser and the SPP leads to a fringe pattern with a periodicity of the SPP wavelength in the vicinity of the grating coupler [signature (4) in Figure 1c, note that a systematic numbering of the signatures will be introduced later in the context of the discussion of Figure 2 and is illustrated in Supplementary Figure S1]. However, there is additional contrast further away from the grating coupler, where the laser pulse and the SPP are never present at the same time. Apparently, electrons are emitted in areas where the SPP propagates across the surface. To distinguish the laser-based photoemission from this plasmon-driven electron emission, we will refer to the latter as “plasmoemission”.

Figure 1d,e shows the situation for two linear grating couplers on an atomically flat, single crystalline gold surface (cesiated), where two fs laser pulses that are time-delayed by Δt impinge onto the surface. Each of the laser pulses excites a pair of counter-propagating SPPs at the opposing grating couplers. The 2PPE PEEM images in Figure 1e are acquired at different delay times Δt . For both delays, the same fringe pattern as before (signature 4) appears in the vicinity of the grating couplers. Furthermore, the signature of a transient standing SPP wave is always present in the center between the two couplers (signature 2). The signature of the standing wave pattern exhibits a spatial periodicity of half the SPP wavelength and is spatially well-separated from signature (4). From the latter, we can conclude that electron emission from the transient standing wave is solely caused by the SPPs; signature (2) must thus be ascribed to plasmoemission as well.

After excitation, the SPPs propagate across the surface with almost the speed of light in vacuum. For a delay time of $\Delta t = 33.3$ fs, the SPPs excited by the pump pulse are probed by the second laser pulse after they have propagated ≈ 10 μm , leading to the pump–probe signature of a propagating SPP (signature 3). The fringe spacing of signature (3) resembles the SPP wavelength since the probing occurs with a fixed coherent phase relation and the laser pulses impinge on the surface along the surface normal.³⁴ In contrast to the aforementioned signatures (4) and (2), signature (3) is delay-time dependent.

We will now address the delay-time dependence of the signatures. Figure 2a shows a stack of spatially averaged line profiles taken along the horizontal dashed white line in Figure 1e from 2PPE PEEM images acquired at different delays. In total, eight different measurement signatures, that is, signals with a periodicity in space or delay time, are present. The aforementioned signatures (2)–(4) and their dependence on the time delay are clearly visible (note that the signature labels are shown in the adjacent simulation panel in Figure 2b). Signatures (6)–(8) result from a partial reflection of the SPPs at the opposing grating couplers.

The formation of all signatures and their delay-time dependence can be understood with the help of “space-time diagrams” that illustrate the trajectories of the laser and SPP pulses in (one-dimensional) space x and time t . Figure 2c depicts two of such diagrams for different delays Δt between the pump- and probe pulses (more diagrams for different delay times are given in Supplementary Figure S1). The x coordinate axis is chosen along the horizontal dashed white line in Figure 1e, and the grating couplers are at positions 0 and d . The trajectories of the SPPs excited by the pump- and probe pulse are shown in red and blue, respectively, and the propagation

directions of the SPPs are indicated by arrows. Reflected SPP pulses are indicated by dashed lines. The slope of the SPPs trajectories is determined by the inverse of the SPPs group velocity v_g . The laser pulses are plotted in this representation as horizontal lines at times $t = 0$ and $t = \Delta t$.

The aforementioned signatures are formed, whenever a spatiotemporal overlap of two pulses occurs, which results in an interferometric correlation signal. These situations are indicated by the numbered black dots in Figure 2c. Due to the time integration of the detector, noninterfering (single pulse) contributions to the measurement signal appear as a homogeneous background, featureless in space and delay time. Table 1

Table 1. Classification of the Measurement Signatures

type	spatial periodicity	examples
semipropagating	λ_s	(3), (4), (7)
counter-propagating	$\lambda_s/2$	(2), (5), (8)
copropagating	none	(1), (6)

classifies the different signatures: Semipropagating signatures (3, 4, 7) are formed whenever a SPP interferes with a light pulse; counter-propagating signatures (2, 5, 8) are created by the interference of two counter-propagating SPPs. Copropagating signatures (1, 6) result from the interference of pulses that propagate in the same direction. All three types of signatures exhibit characteristic spatial periodicities (see Table 1). The observation of the novel plasmoemission signatures (2), (5), (6), and (8) poses a paradigm shift in time-resolved surface plasmon-based photoemission microscopy: Up to now, time-resolved imaging of SPPs was accomplished by interfering the surface plasmon waves with a probing laser pulse.²⁵ Here, we observe two different surface plasmon waves probing each other. This plasmoemission-based probing mechanism can be employed, for example, to virtually increase the time-resolution, as is the case for signatures (5) and (8) propagating only with half of the SPPs group velocity $v_g/2$. Furthermore, the plasmoemission signatures provide us with novel insight into the electron emission process as revealed by the following analysis.

Figure 2b shows the result of a numerical simulation in the same representation as the experimental result in Figure 2a. The simulation is based on the known analytical solution of Maxwell’s equations for the electromagnetic fields of the SPPs^{35–37} and the laser pulses. We assume a Gaussian pulse shape and use the relative pulse amplitudes as input parameters. For strong plasmonic fields and normal-incident light, the commonly used yield model for 2PPE PEEM²¹ must be extended to incorporate the out-of-plane electric field component of the SPP as will be discussed below. Following the ansatz of the surface and volume photoelectric effect^{38–40} the 2PPE PEEM yield $Y_{2\text{PPE}}$ in the simulation is calculated using

$$\begin{aligned}
 Y_{2\text{PPE}} \propto & \underbrace{\int (E^{\parallel})^4 dt}_{\text{volume effect}} + \alpha^4 \underbrace{\int (E^{\perp})^4 dt}_{\text{surface effect}} \\
 & + \beta^2 \underbrace{\int (E^{\parallel})^2 \cdot (E^{\perp})^2 dt}_{\text{volume and surface effect}}
 \end{aligned} \quad (1)$$

where E^{\parallel} and E^{\perp} are the (macroscopic) electric field components parallel and perpendicular to the surface resulting from the superposition of all laser-light and SPP contributions, respectively.

The parameters α and β are real numbers. The simulation result shown in Figure 2b has been carried out with $\beta^2/\alpha^2 = 2$ and $\alpha = 5.8$, by considering the fields at the interface inside the metal only [$(E^{\parallel})^2 \approx E^2$, which is proportional to the time-dependent electromagnetic energy density⁴¹].

The yield model given in eq 1 can be validated by an analysis of the standing-wave SPP field, which is formed by the interference of the counter-propagating SPP pulses. The antinodes of the in-plane E_S^{\parallel} and the out-of-plane component E_S^{\perp} of the SPP's electric field are (at all times) spatially separated by $\lambda_S/4$ with respect to each other, as illustrated in Figure 2g. This spatial separation of the electric field components is caused by the opposite transverse spin^{42,43} of the counter-propagating SPP pulses (just like two counter-propagating circularly polarized light pulses of opposite helicity would create a standing wave where s- and p-polarized fields are fixed in space, oscillate in time, and are shifted by a quarter light wavelength with respect to each other). As highlighted by the insets in Figure 2a,b, also the plasmoemission signal (signature 2) is maximal at locations shifted by $\lambda_S/4$ with respect to the locations where the delay-time dependent probing signal (signature 3) is maximal. Since the probing contrast is caused by the interference of the normally incident laser light with the in-plane component of the SPP's electric field,⁴⁴ we conclude that the plasmoemission signal is predominantly governed by the out-of-plane component of the SPPs electric field E_S^{\perp} . This important finding is intimately related to the underlying emission process and motivates an $\alpha > \sqrt{-\epsilon_m/\epsilon_d}$ in the second term in eq 1. Furthermore, the experimental result indicates the occurrence of a mixed volume and surface effect 2PPE process (third term in eq 1). Indeed, all three terms in eq 1 contribute to the observed electron yield, which is confirmed by the simulation results shown in Figure 2b and d–f.

After having shown that plasmoemission is predominantly governed by the *out-of-plane* electric field component rather than the total electromagnetic field density at the surface, we are now going to address the energy transfer from a collective SPP wave to a single electron. To achieve higher SPP field strengths, we employ a circular grating coupler for the focusing of SPPs as sketched in Figure 3a. Again we make use of the SPPs transverse spin to create a transient standing SPP wave (signature 2), in which the SPPs' electric field components E_S^{\parallel} and E_S^{\perp} are spatially separated. Figure 3b shows three energy-filtered electron microscopy images of the plasmoemission focus spot profile of a circular grating coupler (with a diameter of 40 μm) in a thin Ag film under fs laser pulse illumination at zero time-delay. The (minimal order and thus dominating) multiplasmon plasmoemission (MPPE) processes corresponding to the pass energies are indicated in the top left corners of the images. As before, plasmoemission takes place predominantly at locations of maximal E_S^{\perp} . Particularly for the highly nonlinear emission processes this finding becomes even more evident. Figure 3d shows the logarithmically scaled plasmoemission energy spectrum of the emitted electrons obtained from a series of energy-filtered images. The spectrum exhibits edges that are interpreted as replica of the Fermi edge at energies corresponding to multiples of the SPPs energy ($\hbar\omega = 1.55$ eV) and cannot be explained by a nonlinear susceptibility. Indeed, it reveals the quantum nature of the SPP, in analogy to the classical Franck–Hertz experiment from 1911 that demonstrated multiple *quantized energy* ionization steps

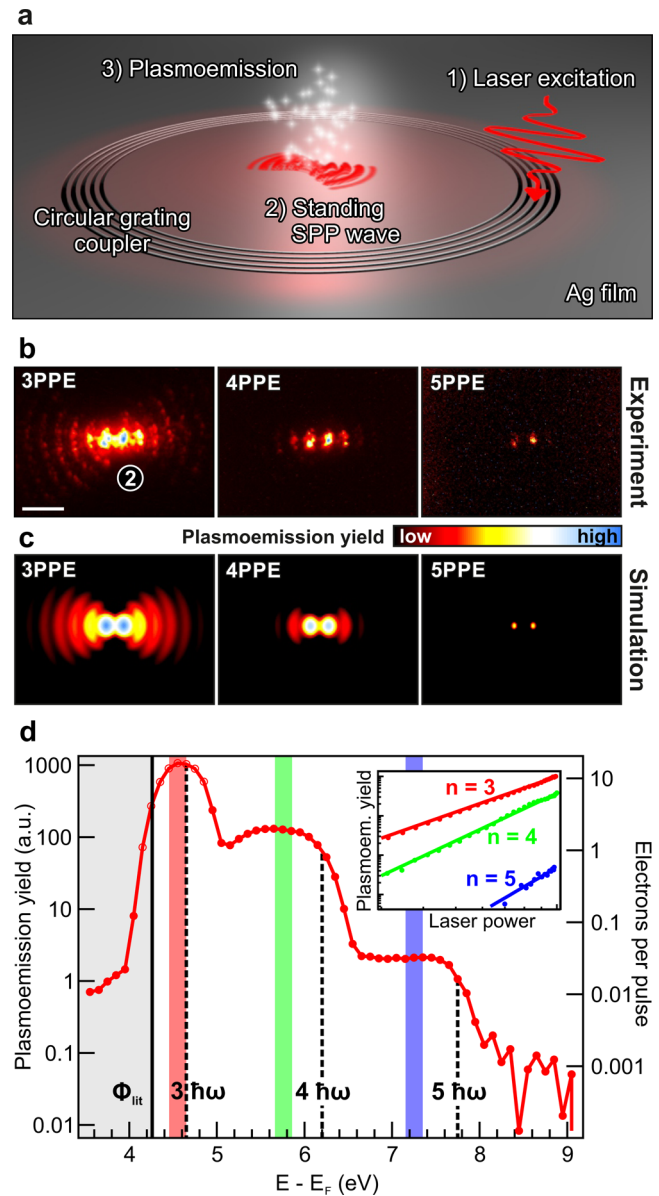


Figure 3. Multiplasmon plasmoemission of electrons from focused surface plasmon polaritons. (a) Sketch. (b) Energy-filtered plasmoemission based electron microscopy images of the focus spot at energies corresponding to different emission orders. Work function $\Phi_{\text{lit}} = 4.26$ eV.⁴⁵ Scale bar: 1 μm . (c) Corresponding simulation results. (d) Plasmoemission energy spectrum. The blank symbols indicate a partial saturation of the detector. Inset: Log–log plot of the plasmoemission yield vs laser power dependencies at the electron energies which are indicated by the vertical colored stripes.

in gases. This interpretation is supported by energy-filtered yield $Y_{n\text{PPE}}$ vs laser power I measurements (inset of Figure 3d), showing characteristic yield dependencies $Y_{n\text{PPE}} \propto I^n$ for multiplasmon processes $n = 3, 4, 5$. To the best of our knowledge, this is the first report of surface plasmon-mediated electron emission up to fifth order from an isolated surface plasmon wave in a defined emission geometry on a flat surface and without the presence of photons.

Notably, the observed power laws follow heuristically from the statistics of a small number of plasmons that is randomly absorbed by a much larger number of electrons. The Poisson distribution states that the probability for an n -th order absorption process is given by $p_n(\xi) = \xi^n/n! \exp(-\xi) \rightarrow \xi^n/n!$

for $\xi \rightarrow 0$, where ξ is the ratio of absorbed plasmons to electrons. The measured yield dependencies and the MPPE PEEM images shown in Figure 3b suggest a generalization of the two-plasmon emission in eq 1 into a n -plasmon version in the form $Y_{n\text{MPPE}} \propto \int \{(E^{\parallel})^2 + \alpha^2(E^{\perp})^2\}^n dt$ with $\beta^2/\alpha^2 = 2$ from the previous analysis. Figure 3c shows corresponding simulations of the MPPE plasmoemission patterns in the focus region (more details of the simulation method are given in ref 46). The simulation results are in good agreement with the measurements, apart from a small Ag surface roughness related spatial yield modulation.

In conclusion, our time-resolved imaging experiments illustrate that emission of electrons from a plasmonic field can be the dominant contribution in photoemission experiments. By separating fs laser pulses from fs SPP pulses in space and time, we were able to disentangle light-induced photoemission and nonlinear plasmoemission on flat metallic surfaces. By exploiting the opposite transverse spin of two counter-propagating SPPs, we were able to spatially separate the SPPs electric field components. For normal-incident light, the pump-probe signal of a propagating SPP is caused by the volume effect, while plasmoemission is dominated by the surface effect, motivating an extended yield model. In strong transient standing-wave SPP fields, we observe multiplasmon electron emission up to the fifth order from a flat surface, indicating how effective the plasmonic electron emission pathway is. The experiments reflect the quantum mechanical nature of the SPPs: The plasmoemission probability is determined by the macroscopic electromagnetic field, whereas energy is transferred in quanta of the SPPs energy.

Methods. The experiments were performed in a spectroscopic low-energy electron microscope⁴⁷ (SPE-LEEM III) from Elmitec GmbH. The ultrahigh vacuum (UHV) microscope with a base pressure of $<1 \times 10^{-10}$ mbar is combined with a femtosecond Ti:sapphire laser oscillator (Femtolasers) for two photon photoemission experiments. The laser system provides us with <15 fs short laser pulses at a central wavelength of 800 nm at a repetition rate of 80 MHz. For time-resolved measurements, pump- and probe pulses were created in a home-built Pancharatnam phase-stabilized Mach-Zehnder interferometer.⁴⁸ The general laser setup is described in more detail in an earlier publication.⁴⁹ For imaging SPPs, we use a normal-incidence geometry³⁴ where the laser pulses impinge onto the sample surface along the surface normal.

Polycrystalline, rough Ag thin films (Figure 1c and Figure 3) and single crystalline, atomically flat Au platelets (Figure 1e and Figure 2a) were used as plasmonic materials. The Ag films were evaporated, whereas the Au platelets were produced by a single step thermolysis on the native oxide layer of a Si substrate.⁵⁰ The grating couplers were structured ex-situ via focused ion beam milling (Helios Nanolab 600). Prior to the 2PPE measurements in Figure 1 and Figure 2 a submonolayer amount of cesium was deposited onto the samples from a standard Cs dispenser (SAES Getters) to lower the work function and enable a 2PPE process.

For the simulations in Figure 2b,d-f, eq 1 was calculated by numerical (time) integration using Wolfram Mathematica. The values for the phase and group velocity of the SPP wave packets were calculated from literature values for the dielectric function of gold.⁵¹ The electric field components were considered at the interface inside the metal only. The total electric field \vec{E} at the interface consists of the pump- and probe laser pulse, \vec{E}_{L1} and \vec{E}_{L2} , and the SPPs excited by the two laser pulses, \vec{E}_{S1} and \vec{E}_{S2} ,

respectively: $\vec{E} = \vec{E}_{L1} + \vec{E}_{S1} + \vec{E}_{L2} + \vec{E}_{S2}$. For the situation of two linear grating couplers, each laser pulse, $i = 1,2$, excites an SPP at the left (l) and the right (r) grating coupler, and partial reflection (ref) of each excited SPP at the opposed grating coupler takes place, thus $\vec{E}_{S,i} = \vec{E}_{S,i}^l + \vec{E}_{S,i}^r + \vec{E}_{S,i}^{l,\text{ref}} + \vec{E}_{S,i}^{r,\text{ref}}$. The amplitudes of the excited SPPs $E_{S,i}^{j,\parallel}$, $j = l,r$, and the reflected ones $E_{S,i}^{j,\text{ref},\parallel}$ were chosen as $E_{S,i}^{j,\parallel}/0.3 = E_{S,i}^{j,\text{ref},\parallel}/0.06 = E_L$ (for an excitation at each of the five grooves), where E_L is the electric field strength of the laser at the interface.

■ ASSOCIATED CONTENT

Supporting Information

The Supporting Information is available free of charge on the ACS Publications website at DOI: 10.1021/acs.nanolett.7b02235.

Space-time diagrams at different delay-times illustrating the formation of all observed measurement signatures (1–8) (PDF)

■ AUTHOR INFORMATION

Corresponding Author

*E-mail: meyerzh@uni-due.de.

*E-mail: daniel.podbiel@uni-due.de.

ORCID

Daniel Podbiel: 0000-0002-6592-4146

Timothy J. Davis: 0000-0002-7299-4900

Present Address

S.S.: Infineon Technologies AG, 59581 Warstein, Germany.

Notes

The authors declare no competing financial interest.

■ ACKNOWLEDGMENTS

Financial support from the Deutsche Forschungsgemeinschaft through SFB 616 “Energy Dissipation at Surfaces”, SPP 1391 “Ultrafast Nano-optics”, and CRC 1242 “Non-Equilibrium Dynamics of Condensed Matter in the Time Domain” as well as ERC (Complexplas), BMBF, Zeiss-Stiftung, and BW Stiftung is gratefully acknowledged. T.J.D. gratefully acknowledges support from University of Stuttgart and Max-Planck-Institute for Solid State Research.

■ REFERENCES

- Petek, H.; Ogawa, S. *Prog. Surf. Sci.* **1997**, *56*, 239–310.
- Höfer, U.; Shumay, I. L.; Reuß, Ch.; Thomann, U.; Wallauer, W.; Fauster, Th. *Science* **1997**, *277*, 1480–1482.
- Echenique, P.; Berndt, R.; Chulkov, E.; Fauster, T.; Goldmann, A.; Höfer, U. *Surf. Sci. Rep.* **2004**, *52*, 219–317.
- Güdde, J.; Rohleder, M.; Meier, T.; Koch, S.; Höfer, U. *Science* **2007**, *318*, 1287–1291.
- Bovensiepen, U.; Petek, H.; Wolf, M. *Dynamics at solid state surfaces and interfaces: Current developments*; Wiley-VCH, 2010.
- Tsang, T.; Srinivasan-Rao, T.; Fischer, J. *Phys. Rev. B: Condens. Matter Mater. Phys.* **1991**, *43*, 8870–8878.
- Aeschlimann, M.; Schmuttenmaer, C. A.; Elsayed-Ali, H. E.; Miller, R. J. D.; Cao, J.; Gao, Y.; Mantell, D. A. *J. Chem. Phys.* **1995**, *102*, 8606–8613.
- Herink, G.; Solli, D. R.; Gulde, M.; Ropers, C. *Nature* **2012**, *483*, 190–193.
- Dombi, P.; Irvine, S. E.; Racz, P.; Lenner, M.; Kroo, N.; Farkas, G.; Mitrofanov, A.; Baltuska, A.; Fuji, T.; Krausz, F.; Elezabi, A. Y. *Opt. Express* **2010**, *18*, 24206–24212.

- (10) Racz, P.; Irvine, S. E.; Lenner, M.; Mitrofanov, A.; Baltuska, A.; Elezzabi, A. Y.; Dombi, P. *Appl. Phys. Lett.* **2011**, *98*, 111116–3.
- (11) Schertz, F.; Schmelzeisen, M.; Kreiter, M.; Elmers, H.-J.; Schönhense, G. *Phys. Rev. Lett.* **2012**, *108*, 237602–5.
- (12) Schenk, M.; Krüger, M.; Hommelhoff, P. *Phys. Rev. Lett.* **2010**, *105*, 257601–4.
- (13) Schröder, B.; Sivis, M.; Bormann, R.; Schäfer, S.; Ropers, C. *Appl. Phys. Lett.* **2015**, *107*, 231105.
- (14) Müller, M.; Kravtsov, V.; Paarmann, A.; Raschke, M.; Ernstorfer, R. *ACS Photonics* **2016**, *3*, 611–619.
- (15) Specht, M.; Pedarnig, J. D.; Heckl, W. M.; Hansch, T. W. *Phys. Rev. Lett.* **1992**, *68*, 476–479.
- (16) Sandtke, M.; Engelen, R.; Schoenmaker, H.; Attema, I.; Dekker, H.; Cerjak, I.; Korterik, J.; Segerink, F.; Kuipers, L. *Rev. Sci. Instrum.* **2008**, *79*, 013704.
- (17) Drezet, A.; Hohenau, A.; Koller, D.; Stepanov, A.; Ditzbacher, H.; Steinberger, B.; Aussenegg, F.; Leitner, A.; Krenn, J. *Mater. Sci. Eng., B* **2008**, *149*, 220–229.
- (18) Gorodetski, Y.; Chervy, T.; Wang, S.; Hutchison, J.; Drezet, A.; Genet, C.; Ebbesen, T. W. *Optica* **2016**, *3* (1), 48–53.
- (19) Hachtel, J. A.; Davidson, R. B., II; Chisholm, M. F.; Lawrie, B. J.; Haglund, R. F., Jr.; Pantelides, S. T. *Microsc. Microanal.* **2016**, *22*, 266–267.
- (20) Kubo, A.; Onda, K.; Petek, H.; Sun, Z.; Jung, Y.; Kim, H. *Nano Lett.* **2005**, *5*, 1123–1127.
- (21) Kubo, A.; Pontius, N.; Petek, H. *Nano Lett.* **2007**, *7*, 470–475.
- (22) Meyer zu Heringdorf, F. J.; Chelaru, L. I.; Möllenbeck, S.; Thien, D.; Horn-von Hoegen, M. *Surf. Sci.* **2007**, *601*, 4700–4705.
- (23) Lemke, C.; Leissner, T.; Jauernik, S.; Klick, A.; Fiutowski, J.; Kjelstrup-Hansen, J.; Rubahn, H.-G.; Bauer, M. *Opt. Express* **2012**, *20*, 12877–12884.
- (24) Lemke, C.; Leißner, T.; Evlyukhin, A.; Radke, J.; Klick, A.; Fiutowski, J.; Kjelstrup-Hansen, J.; Rubahn, H.; Chichkov, B.; Reinhardt, C.; Bauer, M. *Nano Lett.* **2014**, *14*, 2431–2435.
- (25) Kahl, P.; Podbiel, D.; Schneider, C.; Makris, A.; Sindermann, S.; Witt, C.; Kilbane, D.; Horn-von Hoegen, M.; Aeschlimann, M.; Meyer zu Heringdorf, F. *Plasmonics* **2017**, DOI: 10.1007/s11468-017-0504-6.
- (26) Lemke, C.; Schneider, C.; Leißner, T.; Bayer, D.; Radke, J.; Fischer, A.; Melchior, P.; Evlyukhin, A.; Chichkov, B.; Reinhardt, C.; Bauer, M.; Aeschlimann, M. *Nano Lett.* **2013**, *13*, 1053–1058.
- (27) Könenkamp, R.; Word, R. C.; Fitzgerald, J. P. S.; Nadarajah, A.; Saliba, S. D. *Appl. Phys. Lett.* **2012**, *101*, 141114.
- (28) Meyer zu Heringdorf, F.; Podbiel, D.; Raß, N.; Makris, A.; Buckanie, N.; Kahl, P. *Proc. SPIE* **2016**, 9921, 992110.
- (29) Dabrowski, M.; Dai, Y.; Argondizzo, A.; Zou, Q.; Cui, X.; Petek, H. *ACS Photonics* **2016**, *3*, 1704–1713.
- (30) Word, R. C.; Dornan, T.; Könenkamp, R. *Appl. Phys. Lett.* **2010**, *96*, 251110.
- (31) Frank, B.; Kahl, P.; Podbiel, D.; Spektor, G.; Orenstein, M.; Fu, L.; Weiss, T.; Horn-von Hoegen, M.; Davis, T.; Meyer zu Heringdorf, F.; Giessen, H. *Sci. Adv.* **2017**, *3*, e1700721–9.
- (32) Spektor, G.; Kilbane, D.; Mahro, A.; Frank, B.; Ristok, S.; Gal, L.; Kahl, P.; Podbiel, D.; Mathias, S.; Giessen, H.; Meyer zu Heringdorf, F.; Orenstein, M.; Aeschlimann, M. *Science* **2017**, *355*, 1187–1191.
- (33) Mershdorf, M.; Pfeiffer, W.; Thon, A.; Voll, S.; Gerber, G. *Appl. Phys. A: Mater. Sci. Process.* **2000**, *71*, 547–552.
- (34) Kahl, P.; Wall, S.; Witt, C.; Schneider, C.; Bayer, D.; Fischer, A.; Melchior, P.; Horn-von Hoegen, M.; Aeschlimann, M.; Meyer zu Heringdorf, F. J. *Plasmonics* **2014**, *9*, 1401–7.
- (35) Zayats, A. V.; Smolyaninov, I. I.; Maradudin, A. A. *Phys. Rep.* **2005**, *408*, 131–314.
- (36) Maier, S. A. *Plasmonics Fundamentals and Applications*; Springer, 2007.
- (37) Pitarke, J. M.; Silkin, V. M.; Chulkov, E. V.; Echenique, P. M. *Rep. Prog. Phys.* **2007**, *70*, 1–87.
- (38) Tamm, I.; Schubin, S. *Eur. Phys. J. A* **1931**, *68*, 97–113.
- (39) Endriz, J. G.; Spicer, W. E. *Phys. Rev. B* **1971**, *4*, 4159–4184.
- (40) Feibelman, P. J. *Prog. Surf. Sci.* **1982**, *12*, 287–408.
- (41) Ruppin, R. *Phys. Lett. A* **2002**, *299*, 309–312.
- (42) Bliokh, K. Y.; Smirnova, D.; Nori, F. *Science* **2015**, *348*, 1448–1451.
- (43) Bliokh, K. Y.; Rodriguez-Fortuno, F. J.; Nori, F.; Zayats, A. V. *Nat. Photonics* **2015**, *9*, 796–808.
- (44) Podbiel, D.; Kahl, P.; Meyer zu Heringdorf, F. J. *Appl. Phys. B: Lasers Opt.* **2016**, *122*, 90–6.
- (45) Dweydari, A. W.; Mee, C. H. B. *Phys. Stat. Sol. (a)* **1975**, *27*, 223–230.
- (46) Davis, T. J.; Frank, B.; Podbiel, D.; Kahl, P.; Meyer zu Heringdorf, F.-J.; Giessen, H. *ACS Photonics* **2017**, DOI: 10.1021/acsp Photonics.7b00676.
- (47) Schmidt, T.; Heun, S.; Slezak, J.; Diaz, J.; Prince, K. C.; Lilienkamp, G.; Bauer, E. *Surf. Rev. Lett.* **1998**, *5*, 1287–1296.
- (48) Wehner, M. U.; Ulm, M. H.; Wegener, M. *Opt. Lett.* **1997**, *22*, 1455–1457.
- (49) Meyer zu Heringdorf, F. J.; Kahl, P.; Makris, A.; Sindermann, S.; Podbiel, D.; Horn-von Hoegen, M. *Proc. SPIE* **2015**, 9361, 936110W–8.
- (50) Radha, B.; Arif, M.; Datta, R.; Kundu, T. K.; Kulkarni, G. U. *Nano Res.* **2010**, *3* (10), 738–747.
- (51) Johnson, P. B.; Christy, R. W. *Phys. Rev. B* **1972**, *6*, 4370–4379.